Supplementary
Fig.1

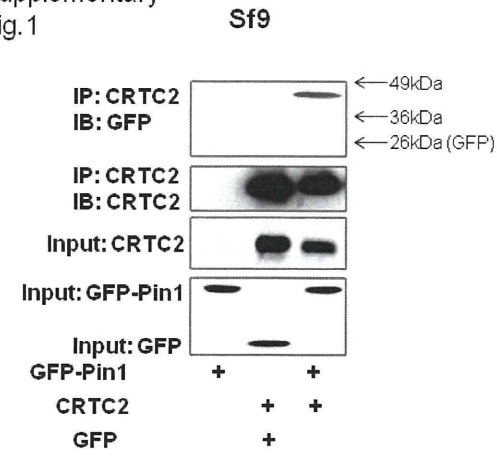

Supplementary
Fig.2

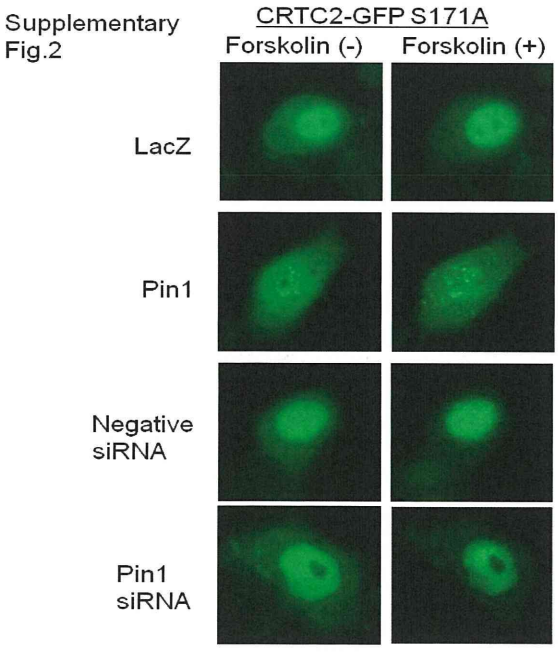

Supplementary Fig.3

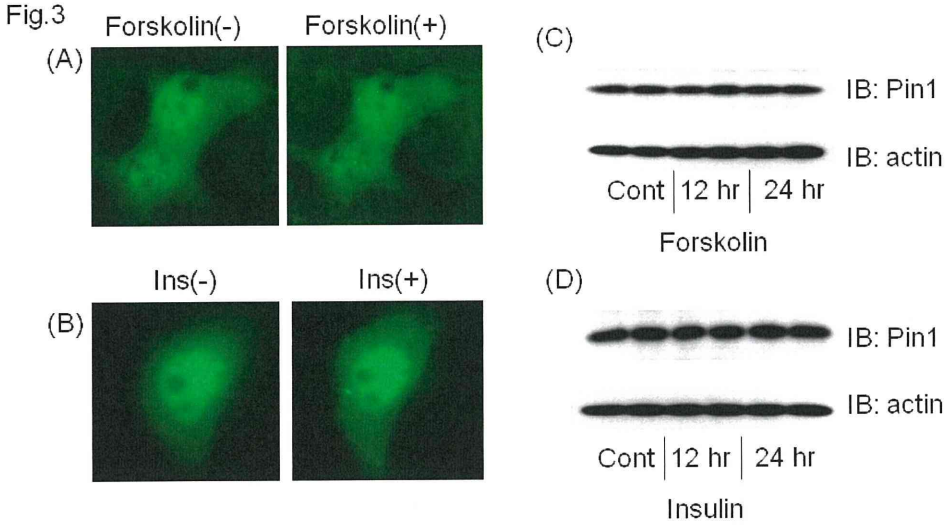

Supplementary Fig. 4

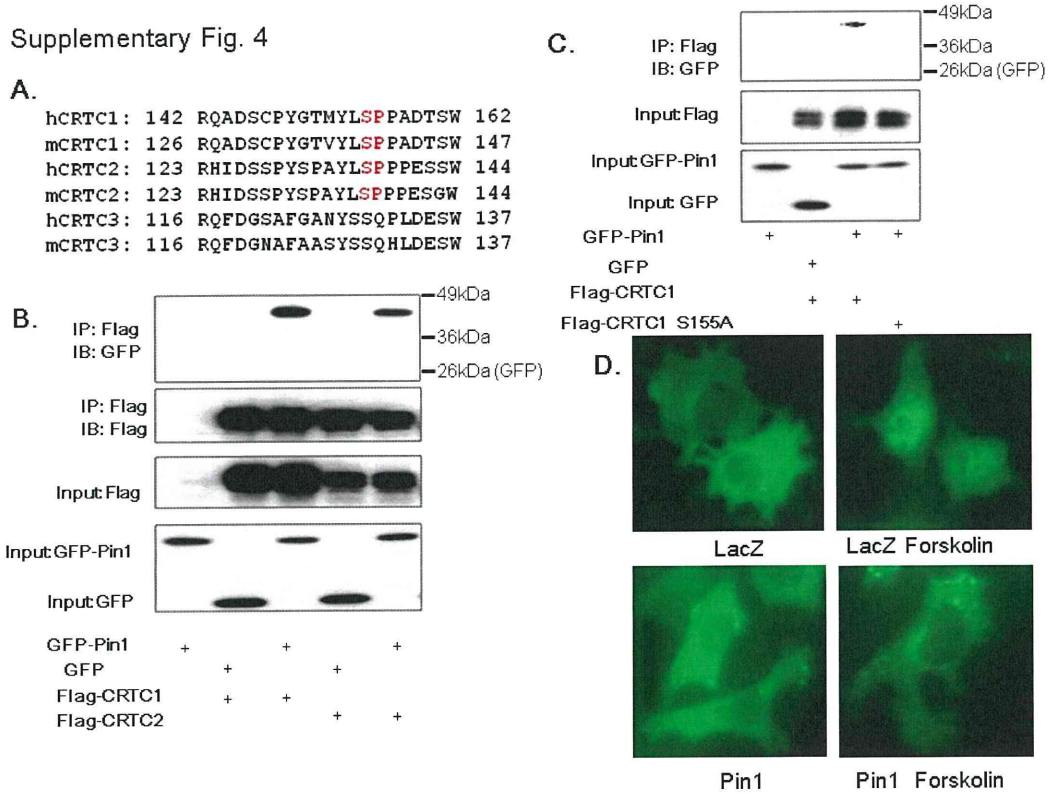

Supplementary
Fig. 5

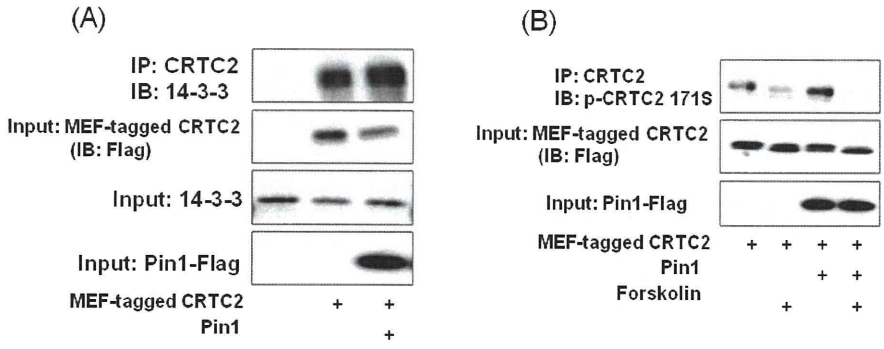

Supplementary
Fig.6

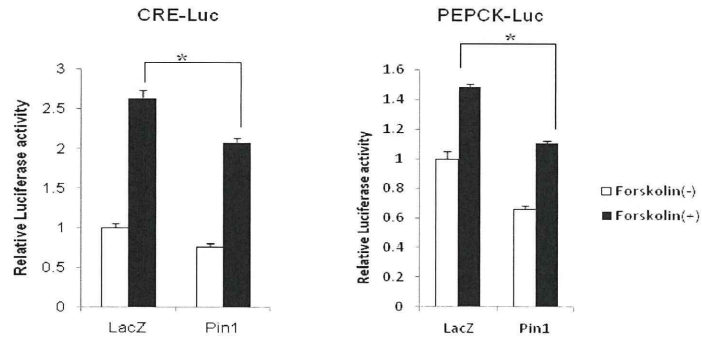

Supplementary
Fig.7

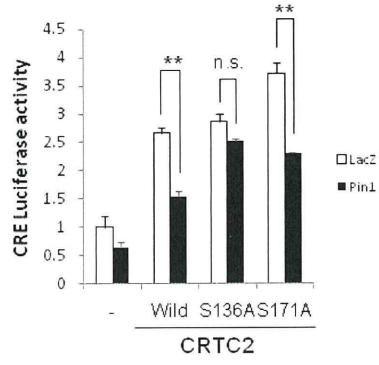

Supplementary
Fig. 8

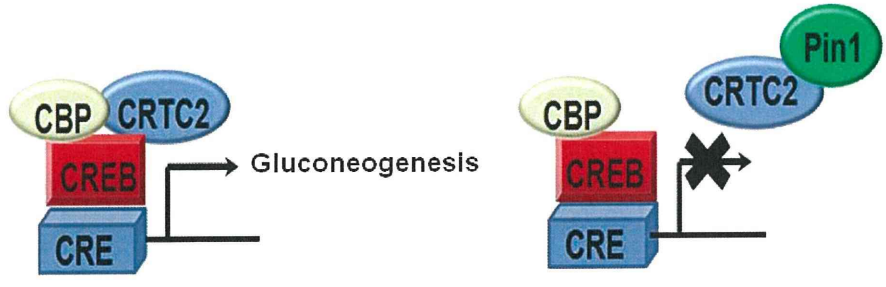

DIABETES RESEARCH AND CLINICAL PRACTICE 87 (2010) 57–63

Contents lists available at ScienceDirect

Diabetes Research and Clinical Practice

journal homepage: www.elsevier.com/locate/diabres

Basic research article

Macrophage foam cell formation is augmented in serum from patients with diabetic angiopathy

Xinglong Cui[a], *Akifumi Kushiyama*[b], *Masayasu Yoneda*[a], *Yusuke Nakatsu*[a], *Ying Guo*[a], *Jun Zhang*[a], *Haruya Ono*[a], *Machi Kanna*[a], *Hideyuki Sakoda*[c], *Hiraku Ono*[d], *Takako Kikuchi*[b], *Midori Fujishiro*[c], *Masashi Shiomi*[e], *Hideaki Kamata*[a], *Hiroki Kurihara*[f], *Masatoshi Kikuchi*[b], *Shoji Kawazu*[b], *Fusanori Nishimura*[g], *Tomoichiro Asano*[a,*]

[a] *Department of Medical Chemistry, Division of Molecular Medical Science, Graduate School of Biomedical Science, Hiroshima University, 1-2-3 Kasumi, Minami-ku, Hiroshima City, Hiroshima, Japan*

[b] *The Institute for Adult Diseases, Asahi Life Foundation, 1-6-1 Marunouchi, Chiyoda-ku, Tokyo, Japan*

[c] *Department of Internal Medicine, Graduate School of Medicine, University of Tokyo, 7-3-1 Hongo, Bunkyo-ku, Tokyo, Japan*

[d] *Department of Medicine, Diabetes Research Center, Albert Einstein College of Medicine, New York, NY, USA*

[e] *Institute for Experimental Animals, Kobe University School of Medicine, Kobe, Hyogo, Japan*

[f] *Physiological Chemistry and Metabolism, Graduate School of Medicine, University of Tokyo, Bunkyo-ku, Tokyo, Japan*

[g] *Department of Dental Science for Health Promotion, Division of Cervico-Gnathostomatology, Graduate School of Biomedical Sciences, Hiroshima University, Japan*

ARTICLE INFO

Article history:
Received 3 April 2009
Received in revised form
18 October 2009
Accepted 22 October 2009
Published on line 24 November 2009

Keywords:
Macrophage
Diabetic angiopathy
Ex vivo assay
Foam cell

ABSTRACT

The differentiation of macrophages into cytokine-secreting foam cells plays a critical role in the development of diabetic angiopathy. J774.1, a murine macrophage cell line, reportedly differentiates into foam cells when incubated with oxidized LDL, ApoE-rich VLDL or WHHLMI (myocardial infarction-prone Watanabe heritable hyperlipidemic) rabbit serum. In this study, serum samples from Type 2 diabetic patients were added to the medium with J774.1 cells and the degree of foam cell induction was quantified by measuring lipid accumulation. These values were calculated relative to the activities of normal and WHHLMI rabbit sera as 0% and 100%, respectively, and termed the MMI (Macrophage Maturation Index). These MMI values reflected intracellular lipids, including cholesteryl ester assayed by GC/MS. Statistical analysis revealed MMI to correlate positively and independently with serum triglycerides, the state of diabetic retinopathy, nephropathy and obesity, but negatively with administration of α-glucosidase inhibitors or thiazolidinediones. Taken together, our results suggest that this novel assay may be applicable to the identification of patients at risk for rapidly progressive angiopathic disorders.

* *Corresponding author*. Tel.: +81 332016781; fax: +81 332016881.
E-mail address: asano-tky@umin.ac.jp (T. Asano).

Abbreviations: BS, blood sugar; sBP, systolic blood pressure; dBP, diastolic blood pressure; TC, total cholesterol; TG, triglyceride; SU, sulfonylurea; α-GI, α-glucosidase inhibitor; BG, Biguanide; TZD, thiazolidinedione; eGFR, estimated glomerular filtration ratio; GC, gas chromatography; AUC, area under the curve.

0168-8227/$ – see front matter
doi:10.1016/j.diabres.2009.10.011

1. Introduction

Macrophages play important roles in the progression of both diabetic microangiopathy [1,2] and macroangiopathy [3–5]. Macrophages invade the dysfunctional vascular endothelium, change into foam cells by taking up lipids, and secrete high levels of several inflammatory hormones, as well as matrix metalloproteases, which contribute to the development of pathological lesions and remodeling. Indeed, foam cells appear even in the early stages of angiopathy, and the accumulation of large numbers of foam cells is often observed in advanced lesions.

Considering that numbers of patients with diabetic angiopathy and metabolic syndrome are rising dramatically worldwide, it is important to develop a method of identifying those with rapidly progressive angiopathic lesions. In this study, we measured patient serum activity inducing the differentiation of J774.1 into foam cells. During foam cell formation from macrophages, numerous factors including oxidized LDL play an enhancing role [6,7], but J774.1 cells reportedly differentiate into foam cells when incubated with oxidized low density lipoprotein (LDL), very low density lipoprotein (VLDL), or myocardial infarction-prone Watanabe heritable hyperlipidemic (WHHLMI) rabbit serum [8]. The WHHLMI rabbit was developed from WHHL rabbits [9], which have a mutated LDL receptor and hypercholesterolemia, such that atherosclerosis develops rapidly [10,11]. The incidence of myocardial infarction in WHHL rabbits was low, while WHHLMI rabbits developed coronary occlusion and spontaneous myocardial infarction reportedly due to having higher amounts of apolipoprotein E-rich VLDL [12–14].

We investigated whether serum activities in diabetic patients inducing the differentiation of J774.1 cells into foam cells, differ according to patient features including metabolic control, development of angiopathic complications, drug treatments, and so on. Our statistical analysis revealed that foam cell-inducing activity correlates positively and independently with serum triglycerides (TG), the state of diabetic retinopathy, nephropathy and obesity, but negatively with administration of α-glucosidase inhibitors (α-GI) or thiazolidinediones (TZD). Such an assay was thus suggested to possibly be applicable to identifying patients at risk for rapidly progressing angiopathic disorders.

2. Materials and methods

2.1. Reagents and cell culture

Murine macrophage-like J774.1 cells were purchased from Riken (Tsukuba, Japan), cultured in RPMI 1640 (Sigma) medium supplemented with 10% fetal calf serum (FCS) (Invitrogen), Penicillin 100 U/ml and Streptomycin 100 μg/ml (GIBCO Invitrogen) at 37 °C in 5% CO_2. All reagents were of analytical grade.

Cells were cultured on 96 well plates (IWAKI) for serum stimulation and lipid accumulation assays. At 90% confluence, each well was incubated with serum free RPMI1640 for 24 h, and then stimulated with 2% serum from individual patients for 72 h. The cells were then subjected to lipid accumulation

Table 1 – (a) Coefficients of correlation and their significance for parametric variables and MMI. (b) Means of MMI for all groups classified by non-parametric complications and use of medications. Values are given as means ± SE. (c) Partial regression coefficients and their significances, for variables adjusted for each other but not normalized. Significance is represented by the *p* values at the bottom.

	Coefficients	*p* value
a.		
Age	−0.025	0.827
BS	0.249	0.030*
HbAlc	0.254	0.027*
sBP	0.068	0.562
dBP	0.075	0.518
WBC	0.246	0.032*
AST	0.012	0.917
ALT	0.134	0.248
γGTP	0.146	0.208
TC	−0.077	0.507
HDL	−0.509	2.55×10^{-6}***
TG	0.528	9.68×10^{-7}***
BMI	0.257	0.025*
Cre	0.259	0.024*
eGFR	−0.188	0.104
	−	+
b.		
Gender (M/F)	19.27 ± 4.97	13.33 ± 1.24
Retinopathy	13.18 ± 1.38	26.07 ± 7.54**
Proteinuria	12.05 ± 1.14	25.46 ± 5.91*
IHD	15.35 ± 1.82	11.55 ± 3.09
SU	14.47 ± 2.57	15.69 ± 2.18
α-GI	15.83 ± 2.03	12.12 ± 2.61
TZD	14.80 ± 1.82	17.88 ± 3.10
BG	12.03 ± 1.25	20.85 ± 4.14*
Insulin	13.10 ± 1.57	18.79 ± 3.87
Anti-RA	11.09 ± 1.11	20.54 ± 3.52*
Statin	13.13 ± 1.27	18.73 ± 4.27
Anti-platelet	14.43 ± 0.96	22.22 ± 15.36
	Coefficients	*p* value
c.		
(Intercept)	19.55	0.544
Age	−0.282	0.029*
BS	0.005	0.869
HbAlc	−1.211	0.388
sBP	0.072	0.286
dBP	−0.129	0.231
WBC	0.043	0.560
AST	0.324	0.140
ALT	−0.196	0.179
γGTP	0.005	0.938
TC	−0.086	0.022*
HDL	0.046	0.593
TG	0.088	3.66×10^{-8}***
BMI	0.590	0.099†
Cre	0.496	0.952
eGFR	0.002	0.986
Gender	0.307	0.926
Retinopathy	9.304	0.029*
Proteinuria	9.363	0.017*
IHD	−7.429	0.152
CVD	3.128	0.728
SU	−1.551	0.541
α-GI	−6.307	0.018*

Table 1 (*Continued*)

	Coefficients	*p* value
TZD	−8.273	0.158
BG	4.333	0.088†
Insulin	−1.578	0.637
Anti-RA	−0.641	0.802
Statin	0.789	0.748
Anti-platelet	−4.185	0.312

* $p < 0.05$.
** $p < 0.01$.
*** $p < 0.001$.
† $p < 0.1$.

assays using AdipoRed (Cambrex), according to the manufacturer's instructions [15]. In brief, the cells were carefully rinsed with phosphate buffered saline (PBS), and 5 μl of AdipoRed reagent were then added to 200 μl of PBS, followed incubation for 10 min at room temperature. Fluorescence was measured with excitation and emission wavelengths of 485 nm and 572 nm, respectively, by fluorimetry. The value obtained with 2% WHHLMI rabbit serum incubation was taken as the Macrophage Maturation Index (MMI) of 100, while 2% normal rabbit serum incubation yielded an MMI of zero. A calibration curve was obtained by serial dilutions of WHHLMI with normal serum. One raw value was the mean, in relative fluorescence units, of five areas per well, and assays were performed five times to obtain a mean MMI value.

2.2. *Serum sampling*

The subjects were 76 patients (53 males and 23 females), who underwent serum sampling in hospitals affiliated with the Institute for Adult Disease, Asahi Life Foundation. The blood examination data and clinical presentations of patients, obtained in routine clinical practice, were collected at the same time as serum sampling. Stage of diabetic retinopathy was determined within 12 months prior to blood sampling, and stage at the last fundus examination was adopted if several examinations had been performed due to stage instability during the prior 12-month period. Patient characteristics are presented in Table 1. All subjects gave informed consent and the study was verified by the institutional ethics committee.

2.3. *Lipid extraction, purification, and separation by GC/MS*

To analyze lipid profiles of accumulated intracellular lipids in J774.1 cells, total lipids were extracted and purified by the Folch method, as previously described [16]. Then, the lipids were dissolved in *n*-hexane and 1 μl of sample was injected into an RTX-5MS (0.25 mm ID × 30 m, 0.25 μm) column attached to a gas chromatograph (Thermo Finnigan Trace GC 2000) which was connected to a mass spectrometer (Thermo Finnigan Trace MS: scanning range: 1–600 *m/z*). The injection temperature was 250 °C, and oven temperatures were 100 °C (2 min) → (25 °C/min) → 250 °C (20 min) → (10 °C/min) → 270 °C (10 min). Cholesteryl components were detected at 362–368 *m/z* independently of other substances.

2.4. *Statistical analysis*

We quantified non-parametrical data such as type of medication, and the state of diabetic complications into indicator variables. Diabetic neuropathy was not assessed because of its variable clinical presentations, which cannot be quantified adequately for transformation into a simple dummy variable and thus could not be effectively utilized in the relatively small number of subjects in this study. Diabetic retinopathy was initially recorded using the Fukuda Classification [17], and stage A2 or later on the most severely affected side, *i.e.* active and progressive states of retinopathy, were dummied as 1, others as 0. Stage of diabetic nephropathy was omitted because diagnosing nephropathy by estimated glomerular filtration ratio (eGFR) and proteinuria was deemed redundant. The presence of ischemic heart disease (IHD) and/or cardiovascular disease (CVD) was determined based on past events, or past and ongoing therapies for these disorders. All ongoing medical therapy classified in Table 1 was dummied as 1 and others 0, dosage-independently.

Data organizing was achieved with Excel2000 (Microsoft), and hierarchical cluster analysis, described using GENESIS 1.7.2 (IGB-TUG). Other statistical analyses were performed using R 2.6.2 (The R Foundation for Statistical Computing), *i.e.* one-way ANOVA, principal component analysis, multi-regression analysis and logistic regression analysis. The Akaike information criterion (AIC) was used to select the best of a collection of candidate models for this dataset.

3. Results

3.1. *Macrophage Maturation Index*

In the macrophage cell line J774.1, administering WHHLMI rabbit serum (final conc. 2%) time-dependently increased macrophage foaming, and lipid accumulation was observed (Fig. 1a) and quantified (Fig. 1b). WHHLMI rabbits exhibit hypercholesterolemia and hypertriglyceridemia, and develop atherosclerosis spontaneously *in vivo* [9]. Their serum thus has the capacity to induce macrophage foaming *ex vivo*. We termed the relative value of lipid accumulation at 72 h, standardized by serial dilution of serum from a WHHLMI rabbit, the MMI. The intra-assay coefficient of variation (CV) was 5.60% ($n = 8$) and the inter-assay CV was 9.43% ($n = 6$). This bioassay was affected by the status of the J774.1 cell line. Thus, assays must be performed with careful attention to cell viability.

We next investigated the MMI of Type 2 diabetic patients whose characteristics are presented in Table 1, and obtained a value of 15.02 ± 14.76 (Supple. 1).

3.2. *Mining the MMI and other datasets*

To clarify the relationships between MMI and other variables, we obtained sera from patients undergoing routine medical investigations. We organized and applied the data to the following analysis. As shown in Fig. 2a, data from all patients were normalized by variables and aligned in ascending order of MMI values. Herein, a tendency for clinical presentation

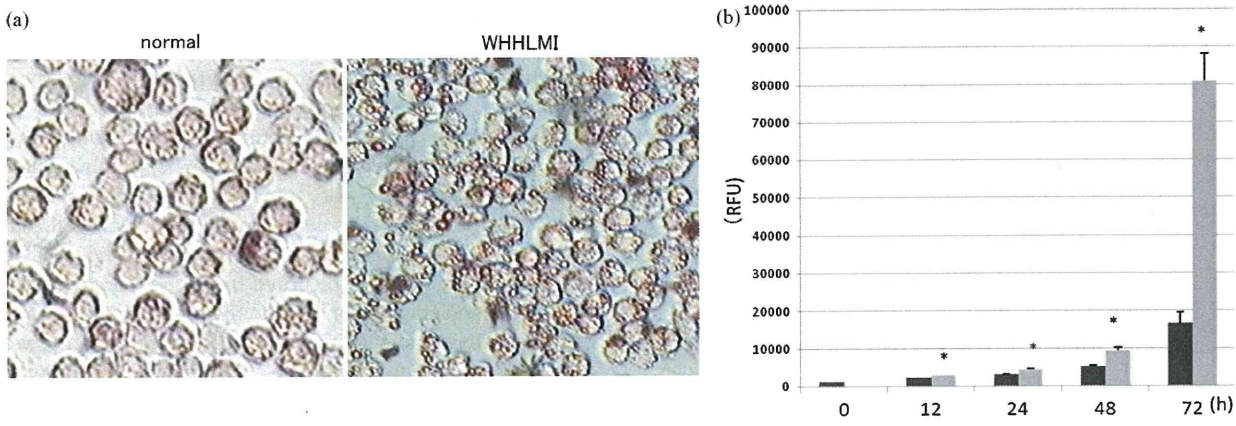

Fig. 1 – (a) Murine macrophage-like cell foaming and lipid accumulation. Cells were cultured on 96-well plates for serum stimulation and lipid accumulation assays. At 90% confluence, each well was incubated with serum free medium for 24 h, and then stimulated with 2% serum from normal and WHHLMI rabbits for 72 h. The cells were then subjected to lipid accumulation assays using Oil red O staining for presentation as an optical microscope image, and using AdipoRed (Cambrex) for quantification. (b) Quantification of lipid accumulation in a time-dependent manner. The cells were carefully rinsed with PBS, and 5 μl of AdipoRed reagent were then added to 200 μl of PBS, followed by incubation for 10 min at room temperature. Fluorescence was measured with excitation and emission wavelengths of 485 nm and 572 nm, respectively, by fluorimetry. One raw value served as the mean of the relative fluorescence, in units, of five areas. The assays were performed five times to obtain a mean MMI value.

with a high MMI to correlate with high Cre, HbA1c, proteinuria and diabetic retinopathy was already apparent, while a low MMI reflected α-GI administration. In Fig. 2b, hierarchical clustering of variables is shown. MMI clustered with TG and renal function. Other variables showed clustering with each other. Only two subjects had CVD, such that power was inadequate for significant variables to be identified by any test. Thus, subjects with CVD were included among those with IHD.

MMI and originally parametric variables are presented in Table 1a. Significant correlations existed between MMI and variables concerning blood glucose control (BS, HbA1c), the inflammatory state (WBC), lipid profile (HDL, TG) and renal function (Cre). When MMI was classified by groups of complications or medications administered, formed retinopathy, proteinuria and administration of BG and anti-RA were associated with significantly higher MMI. Only α-GI administration tended to be associated with lower MMI. With MMI as a criterion variable and others as predictor variables, partial coefficients for regression were calculated, as shown in Table 1c. There was an independent relation between MMI and each variable. Some variables showed inverse correlations or differing significance for the datasets in Table 1a and c, and

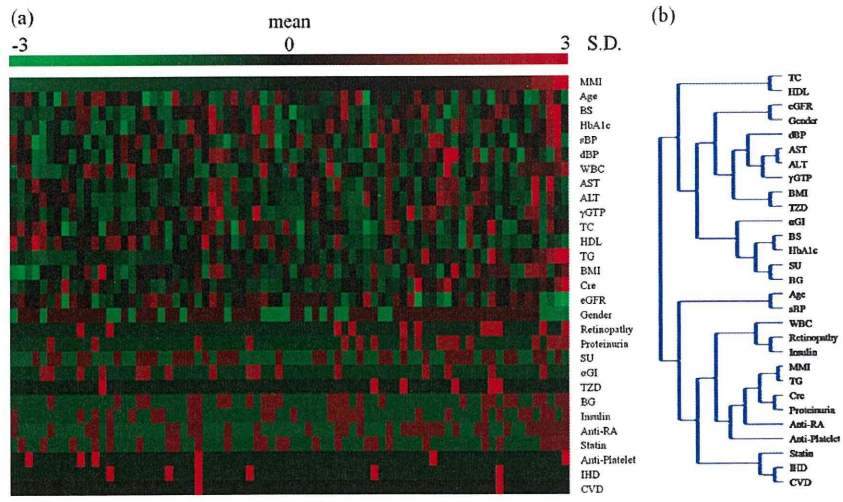

Fig. 2 – (a) Optical presentation of all normalized data from subjects. Parameters were normalized by variables and visualized using GENESIS 1.7.2. Data were aligned in ascending order by MMI from the left for every subject. The tendency was already qualitatively apparent. (b) Hierarchical clustering analysis of variables. Variables presented similar patterns, being clustered in one neighborhood.

Table 2 – Model for multiple regression analysis. Variables were selected by AIC from the variables in Fig. 2. Model: MMI = a × TG (mg/dl) + b × BMI (kg/m^2) + c × (retinopathy) + d × (proteinuria) + e × (α-GI) + f × (TZD) + g.

	Coefficients	Estimated SE	p value
(Intercept)	g −16.97	5.86	0.0051**
TG	a 0.079	0.0076	8.6×10^{-16}***
BMI	b 0.77	0.24	0.0022**
Retinopathy	c 8.79	2.72	0.0019**
Proteinuria	d 8.28	2.23	0.0004***
α-GI	e −7.54	2.24	0.0012**
TZD	f −10.57	3.80	0.0069**

Multiple R^2: 0.75. Adjusted R^2: 0.72.
** $p < 0.01$.
*** $p < 0.001$.

between those in Table 1b and c, probably due to the clinically well-known multi-colinearity (*e.g.* AST and ALT, HDL and TG). In principal component analysis (data not shown), MMI, BS, HbA1c, WBC, HDL, TG, BMI, Cre, retinopathy, proteinuria, BG, Ins, Anti-RA, statin and Anti-Platelet medications were the first principal components.

3.3. *Modeling to account for MMI from routinely obtained parameters*

We subsequently attempted to model a linearly combined collection of variables using stepwise multi-regression analysis. In the model in Table 2, 72% of the variability of MMI was accounted for by variables specified in the model from the adjusted *R*-squared value. Selection of variables was performed using AIC, that is, the relations of MMI to the variables examined in these models were assumed to be stronger than those of residual variables. Values of TG and BMI, the existence of active retinopathy and/or proteinuria, and administrations of α-GI and TZD were determined and their significance was assessed. Coefficients were not standardized in the model, and thus showed gradients for variables reflecting their own measurement units. For instance, a 1 mg/dl rise in TG proportionally indicated an increase of 0.079, diabetic retinopathy an increase of 8.79, and α-GI administration a reduction of 7.54 in MMI. The fitness of the model is described in Supple. 2 as a QQ plot, basically showing a well-fitted and seemingly appropriate model.

TG was the strongest, possibly even excessively influential, variable. However, if our subjects were limited to those with TG values of no more than 300 mg/dl, the TG effect was no longer selected, and BS, AST, HDL and anti-platelet therapy were newly included in the model. BG administration had a reciprocally worsening effect but it was not significant, and diabetic angiopathies and α-GI were still selected, much as in the model shown in Supple. 3. If the strongest TG effect dissipated, 46.51% was still accounted for by the parameters of the adjusted R^2 value despite the smaller subject number.

3.4. *Prediction of diabetic angiopathy activity by MMI*

Sera from patients with both retinopathy and proteinuria exhibited higher MMI than those from patients with either retinopathy or proteinuria (Fig. 3a). To investigate qualitatively whether MMI predicts diabetic angiopathy, a logistic regression analysis was performed (Fig. 3b), using diabetic angiopathy as the criterion variable, and the risk ratio was then estimated. When MMI rose to +1SD (14.76), the risk ratio (RR) for retinopathy was 1.36 (1.10–1.69, 95% C.I.) and the RR adjusted by all other variables was 1.55 (1.06–2.26). The RR for proteinuria was 1.46 (1.18–1.80), the adjusted RR 1.54 (1.10–2.18).

3.5. *Relationships between cholesteryl ester accumulation and MMI*

Relationships of the MMI values and extracted lipid profiles using GC/MS are presented in Supple. 4a and b. In Supple. 4a, a representative GC chart is shown, and the cholesteryl components detected are shown in Supple. 4b. The sum of the AUCs of cholesteryl ester, other lipids (including FFAs, glycerides analyzed from MS data), and total AUCs tended to correlate positively with MMI (Supple. 5).

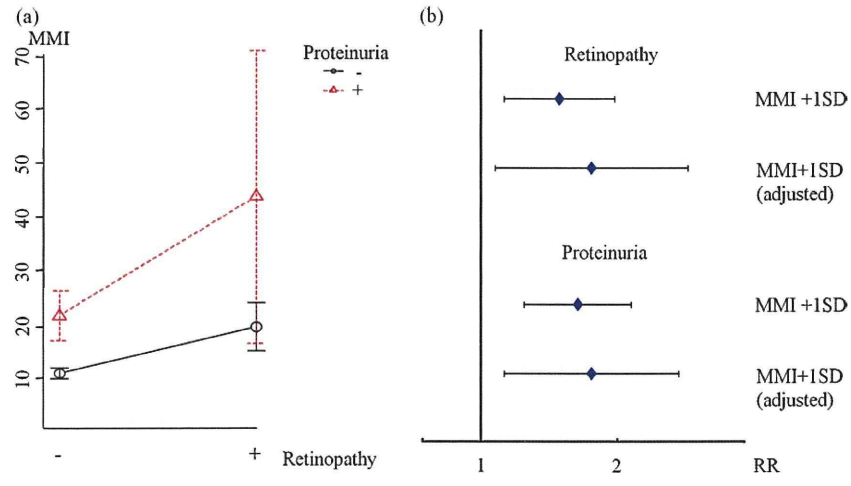

Fig. 3 – (a) Relationships of diabetic angiopathy variables and MMI. Retinopathy and proteinuria together were associated with higher MMI than either retinopathy or proteinuria alone. (b) Risk ratio against increment of MMI (+1SD, 14.76) estimated using logistic regression analysis.

4. Discussion

It is well known that both macroangiopathy and microangiopathy tend to develop rapidly in patients with poorly controlled diabetes. Numerous factors present in macroangiopathy and microangiopathy such as hypertension [18,19], hyperglycemia [20], hyperinsulinemia [21,22], hyperlipidemia [7,23], oxidative stress [24,25] and so on, contribute to angiopathic progression via independent and/or coordinated mechanisms [6,21,24]. Some of these numerous effects act directly on vascular cells [26], while others affect macrophages which invade vascular cells [6]. In this study, we focused on foam cell formation from macrophages, and the activities of patient sera which induce foam cell differentiation were measured. The sera were obtained from diabetic patients, because atherosclerosis and microangiopathy develop rapidly in this patient population. To obtain reproducible values, we used the J774.1 cell line which firmly attaches to culture-dishes and changes into foam cells in response to WHHLMI rabbit serum. Assay reproducibility and validity were confirmed from intra-assay and inter-assay CVs. However, as CVs were still somewhat high, cautious cell handling is critical before proceeding to clinical use. Moreover, by GC analysis, lipid accumulation including cholesteryl ester accumulation rose in proportion to the MMI increase. No specific GC peak corresponding to MMI was detectable. Therefore, the AdipoRed assay precisely reflects intracellular lipid ester accumulation. The obtained values were thus used for comparisons with various clinical factors.

MMI was revealed to be clustered with TG and diabetic nephropathy, the latter being a well-known cause of hypertriglyceridemia [27]. Furthermore, diabetic retinopathy was relatively closely related to MMI and was presumed to be an event preceding nephropathy. Among partial coefficients of regression, age was negative and significant, in fact dovetailing with newly progressive retinopathy being less severe in elderly patients [28].

In multiple regression analysis, we selected six variables which rather strongly accounted for MMI. TG itself is thought to be the primary material of intra-TG accumulation. TZDs might have direct effects against macrophages, while with diabetic retinopathy and nephropathy, administration of an α-GI, which is minimally absorbed from the intestinal tract, and a high BMI reflect only the clinical state and are not directly related to serum parameters. Among these, α-GIs improve blood sugar fluctuations, and a high BMI (obesity) is known to produce metabolic syndrome, the major cause of insulin resistance and atherosclerotic angiopathy. From this viewpoint, it is reasonable that TZDs suppress the ill effects of obesity, by improving insulin resistance. To develop a practical assay, the system shown in the Supple. 3 Table might be worthwhile. It might actually be the case that numerous pathways and bioactive substances affect macrophage maturation in the absence of any lipid effect. Logistic regression analysis, conversely, revealed MMI to be useful for measuring the activity or progression of diabetic angiopathy. In other words, macrophage foam cell formation was related to the development of diabetic microangiopathy. At a minimum, active retinopathy and nephropathy at stage 3a or later were predictable from a higher MMI value at the same time point. Retinopathy and nephropathy acted simply in an additive manner with MMI, suggesting that a higher number of complications reflect the strength of macrophage activity.

Several clinical studies have focused on diabetic angiopathy and medications, with subsets of drugs proving to be effective against angiopathy, though the underlying mechanisms remain uncertain. The α-GIs and TZDs were demonstrated to be effective for the prevention of macrovascular diseases in the stop-NIDDM trial [29] and the PROactive study [30], respectively. However, whether or not this is attributable to direct and/or indirect effects on atherosclerotic regions rather than glycemic control remains unclear. Taking the results of this assay into consideration, these medications may function to prevent macrophage foaming. Moreover, we found that MMI reflected several factors, including foaming or lipid accumulation in individual cells, as well as cell viability and/or growth. Intensive studies focusing on both the characteristics of serum, *i.e.* analysis by 2-DE/mass spectrometry, and the corresponding effects on macrophages, *i.e.* microarray investigations, might clarify the features of macrophage activation.

This study was cross-sectional, such that relationships among variables were ambiguous in terms of cause and effect, especially the impacts of medical therapy. Most of the diabetic patients examined had already received interventional therapies including not only anti-hyperglycemic agents, but also anti-hypertensive agents, statins, anti-coagulants, and so on. Although a future intensive cohort study is needed, MMI might be corrected to avoid excessively strong effects of the lipid state, thus truly reflecting the risk of developing angiopathic diseases in patients with Type 2 diabetes, and thereby become a useful indicator for selecting appropriate medical therapy.

Acknowledgements

We are deeply grateful to Hirokazu Sato and Yuko Oki for their technical supports. This work was supported by a Grant-in-Aid for Exploratory Research from the Japan Promotion of Science Foundation of the Japanese Government.

Appendix A. Supplementary data

Supplementary data associated with this article can be found, in the online version, at doi:10.1016/j.diabres.2009.10.011.

Conflict of interest

There are no conflicts of interest.

REFERENCES

[1] Tesch, Role of macrophages in complications of type 2 diabetes, Clin. Exp. Pharmacol. Physiol. 34 (2007) 1016–1019.
[2] Nguyen, Ping, Mu, Hill, Atkins, Chadban, Macrophage accumulation in human progressive diabetic nephropathy, Nephrology (Carlton) 11 (2006) 226–231.

[3] Boyle, Diabetes mellitus and macrovascular disease: mechanisms and mediators, Am. J. Med. 120 (2007) S12–17.
[4] Simionescu, Implications of early structural-functional changes in the endothelium for vascular disease, Arterioscler. Thromb. Vasc. Biol. 27 (2007) 266–274.
[5] Gacka, Dobosz, Szymaniec, Bednarska-Chabowska, Adamiec, Sadakierska-Chudy, Proinflammatory and atherogenic activity of monocytes in Type 2 diabetes, J. Diabetes Complications (2008).
[6] Hodgkinson, Laxton, Patel, Ye, Advanced glycation end-product of low density lipoprotein activates the toll-like 4 receptor pathway implications for diabetic atherosclerosis, Arterioscler. Thromb. Vasc. Biol. 28 (2008) 2275–2281.
[7] Ishigaki, Katagiri, Gao, Yamada, Imai, Uno, et al., Impact of plasma oxidized low-density lipoprotein removal on atherosclerosis, Circulation 118 (2008) 75–83.
[8] Mori, Itabe, Higashi, Fujimoto, Shiomi, Yoshizumi, et al., Foam cell formation containing lipid droplets enriched with free cholesterol by hyperlipidemic serum, J. Lipid Res. 42 (2001) 1771–1781.
[9] Shiomi, Ito, Yamada, Kawashima, Fan, Development of an animal model for spontaneous myocardial infarction (WHHLMI rabbit), Arterioscler. Thromb. Vasc. Biol. 23 (2003) 1239–1244.
[10] Tanzawa, Shimada, Kuroda, Tsujita, Arai, Watanabe, WHHL-rabbit: a low density lipoprotein receptor-deficient animal model for familial hypercholesterolemia, FEBS Lett. 118 (1980) 81–84.
[11] Buja, Kita, Goldstein, Watanabe, Brown, Cellular pathology of progressive atherosclerosis in the WHHL rabbit. An animal model of familial hypercholesterolemia, Arteriosclerosis 3 (1983) 87–101.
[12] Shiomi, Ito, Shiraishi, Watanabe, Inheritability of atherosclerosis and the role of lipoproteins as risk factors in the development of atherosclerosis in WHHL rabbits: risk factors related to coronary atherosclerosis are different from those related to aortic atherosclerosis, Atherosclerosis 96 (1992) 43–52.
[13] Ishii, Kita, Yokode, Kume, Nagano, Otani, et al., Characterization of very low density lipoprotein from Watanabe heritable hyperlipidemic rabbits, J. Lipid Res. 30 (1989) 1–7.
[14] Ito, Yamada, Shiomi, Progression of coronary atherosclerosis relates to the onset of myocardial infarction in an animal model of spontaneous myocardial infarction (WHHLMI rabbits), Exp. Anim. 53 (2004) 339–346.
[15] Greenspan, Fowler, Spectrofluorometric studies of the lipid probe, nile red, J. Lipid Res. 26 (1985) 781–789.
[16] Kushiyama, Shojima, Ogihara, Inukai, Sakoda, Fujishiro, et al., Resistin-like molecule beta activates MAPKs, suppresses insulin signaling in hepatocytes, and induces diabetes, hyperlipidemia, and fatty liver in transgenic mice on a high fat diet, J. Biol. Chem. 280 (2005) 42016–42025.
[17] Fukuda, Classification and treatment of diabetic retinopathy, Diabetes Res. Clin. Pract. 24 Suppl. (1994) S171–176.
[18] Veglio, Paglieri, Rabbia, Bisbocci, Bergui, Cerrato, Hypertension and cerebrovascular damage, Atherosclerosis (2008).
[19] Silva, Pinto, Biswas, de Faria, de Faria, Hypertension increases retinal inflammation in experimental diabetes: a possible mechanism for aggravation of diabetic retinopathy by hypertension, Curr. Eye Res. 32 (2007) 533–541.
[20] Avogaro, de Kreutzenberg, Fadini, Endothelial dysfunction: causes and consequences in patients with diabetes mellitus, Diabetes Res. Clin. Pract. 82 Suppl. 2 (2008) S94–S101.
[21] Vaidyula, Boden, Rao, Platelet and monocyte activation by hyperglycemia and hyperinsulinemia in healthy subjects, Platelets 17 (2006) 577–585.
[22] Sugimoto, Baba, Suda, Yasujima, Yagihashi, Peripheral neuropathy and microangiopathy in rats with insulinoma: association with chronic hyperinsulinemia, Diabetes Metab. Res. Rev. 19 (2003) 392–400.
[23] Yang, Shi, Hao, Li, Le, Increasing oxidative stress with progressive hyperlipidemia in human: relation between malondialdehyde and atherogenic index, J. Clin. Biochem. Nutr. 43 (2008) 154–158.
[24] Ogihara, Asano, Katagiri, Sakoda, Anai, Shojima, et al., Oxidative stress induces insulin resistance by activating the nuclear factor-kappa B pathway and disrupting normal subcellular distribution of phosphatidylinositol 3-kinase, Diabetologia 47 (2004) 794–805.
[25] Osto, Matter, Kouroedov, Malinski, Bachschmid, Camici, et al., c-Jun N-terminal kinase 2 deficiency protects against hypercholesterolemia-induced endothelial dysfunction and oxidative stress, Circulation 118 (2008) 2073–2080.
[26] Kakehashi, Inoda, Mameuda, Kuroki, Jono, Nagai, et al., Relationship among VEGF, VEGF receptor, AGEs, and macrophages in proliferative diabetic retinopathy, Diabetes Res. Clin. Pract. 79 (2008) 438–445.
[27] Yoshino, Hirano, Nagata, Maeda, Naka, Murata, et al., Hypertriglyceridemia in nephrotic rats is due to a clearance defect of plasma triglyceride: overproduction of triglyceride-rich lipoprotein is not an obligatory factor, J. Lipid Res. 34 (1993) 875–884.
[28] Wong, Molyneaux, Constantino, Twigg, Yue, Timing is everything: age of onset influences long-term retinopathy risk in type 2 diabetes, independent of traditional risk factors, Diabetes Care 31 (2008) 1985–1990.
[29] Chiasson, Josse, Gomis, Hanefeld, Karasik, Laakso, Acarbose for prevention of type 2 diabetes mellitus: the STOP-NIDDM randomised trial, Lancet 359 (2002) 2072–2077.
[30] PROactive study, Lancet 367 (2006) 982.

blood

2010 115: 4138-4147
Prepublished online March 15, 2010;
doi:10.1182/blood-2009-05-223057

Inhibition of endothelial cell activation by bHLH protein E2-2 and its impairment of angiogenesis

Aya Tanaka, Fumiko Itoh, Koichi Nishiyama, Toshiaki Takezawa, Hiroki Kurihara, Susumu Itoh and Mitsuyasu Kato

Blood (print ISSN 0006-4971, online ISSN 1528-0020), is published weekly by the American Society of Hematology, 2021 L St, NW, Suite 900, Washington DC 20036.

Inhibition of endothelial cell activation by bHLH protein E2-2 and its impairment of angiogenesis

Aya Tanaka,[1] Fumiko Itoh,[1] Koichi Nishiyama,[2] Toshiaki Takezawa,[3] Hiroki Kurihara,[2] Susumu Itoh,[1] and Mitsuyasu Kato[1]

[1]Department of Experimental Pathology, Graduate School of Comprehensive Human Sciences, University of Tsukuba, Tsukuba; [2]Department of Physiological Chemistry and Metabolism, Graduate School of Medicine, University of Tokyo, Tokyo; and [3]Transgenic Animal Research Center, National Institute of Agrobiological Sciences, Tsukuba, Japan

E2-2 **belongs to the basic helix-loop-helix (bHLH) family of transcription factors. E2-2 associates with inhibitor of DNA binding (Id) 1, which is involved in angiogenesis. In this paper, we demonstrate that E2-2 interacts with Id1 and provide evidence that this interaction potentiates angiogenesis. Mutational analysis revealed that the HLH domain of E2-2 is required for the interaction with Id1 and vice versa. In addition, Id1 interfered with E2-2–mediated effects on luciferase reporter activities. Interestingly, injection of E2-2–expressing adenoviruses into Matrigel plugs implanted under the skin blocked in vivo angiogenesis. In contrast, the injection of Id1-expressing adenoviruses rescued E2-2–mediated inhibition of in vivo angiogenic reaction. Consistent with the results of the Matrigel plug assay, E2-2 could inhibit endothelial cell (EC) migration, network formation, and proliferation. On the other hand, knockdown of E2-2 in ECs increased EC migration. The blockade of EC migration by E2-2 was relieved by exogenous expression of Id1. We also demonstrated that E2-2 can perturb VEGFR2 expression via inhibition of VEGFR2 promoter activity. This study suggests that E2-2 can maintain EC quiescence and that Id1 can counter this effect. (*Blood*. 2010;115(20): 4138-4147)**

Introduction

Angiogenesis is the formation of new vessels from preexisting ones by sprouting or by intussusceptive microvascular growth. Angiogenesis takes place throughout development as well as in adulthood. Although the vasculature in adults is generally quiescent, angiogenesis occurs to ensure physiologic homeostasis and integrity after wound healing, inflammation, ischemia, and during the female reproductive cycle.[1] Angiogenesis encompasses 2 phases: activation and resolution. The activation phase is initiated by growth factor signals (eg, vascular endothelial growth factor [VEGF], fibroblast growth factor-2 [FGF-2]) or by hypoxia. In this process, endothelial cells (ECs) proliferate, vascular permeability increases, and extracellular matrix components are degraded. These serial events allow ECs to migrate and form new capillary sprouts. During the resolution stage, ECs cease proliferation and migration, the basement membrane is reconstituted, and the vessels mature. The transition from the activation phase to the resolution phase, and vice versa, is referred to as the "angiogenic switch" and is determined by a tightly regulated balance between angiogenic inducers and inhibitors.[2]

The inhibitor of the DNA-binding (Id) family of proteins, consisting of *Id1*, *Id2*, *Id3*, and *Id4*, belongs to the helix-loop-helix (HLH) family of transcription factors. The basic HLH (bHLH) family of transcription factors regulates transcription by binding to DNA as either homodimers or heterodimers. Id proteins, which lack a DNA-binding domain, interact with bHLH proteins to prevent dimer formation and/or DNA binding.[3] In addition, Id1 can associate with members of the Ets protein family and Rb.[4,5] Several observations support a crucial role for Id proteins in development, differentiation, and proliferation of cells, and in tumorigenesis. For example, it has been demonstrated that Id1 can block MyoD-mediated myogenic responses.[6-8] *Id1* and *Id3*, identified as direct targets of bone morphogenetic protein (BMP) signaling,[9-15] are abundantly expressed during blood vessel formation. *Id1/Id3* double-knockout mice display abnormal angiogenesis characterized by enlarged, dilated blood vessels.[16] Introduction of Id1 into ECs induces EC proliferation and migration.[17,18] Because knockdown of Id1 in ECs treated with BMP perturbs EC activation, Id1 is considered to be essential for BMP-induced EC activation.[18] Loss of Id1 in tumor ECs leads to down-regulation of integrin α6, integrin β4, FGFR1, MMP2, and laminin5.[19] Thus, Id1 positively regulates proangiogenic transcripts even though it cannot bind directly to DNA. Although many bHLH transcription factors have been implicated in EC angiogenic activities, which proteins Id1 regulates remains unclear.

We have reported that Hey1/Herp2/Hesr1, one of the bHLH proteins induced by Notch signaling, antagonizes activated BMP receptor-induced EC migration. This antagonism is caused by the degradation of Id1 interacting with Hey1/Herp2/Hesr1 in ECs. Thus, Id1-induced EC migration is blocked by Hey1/Herp2/Hesr1.[20] However, the mechanism by which Id1 triggers EC angiogenic activation is still poorly understood.

To gain more insight into the molecular mechanisms by which Id1 positively regulates EC activation, we searched for Id1 interaction partners using a yeast 2-hybrid system and identified E2-2. E2-2 (also known as ITF2, TCF4, SEF2, and SEF2-1B) is classified into the E-protein family (or the class A type of bHLH transcription factors), whose expression is virtually ubiquitous. In addition to E2-2, *E2A* and *HEB* also belong to the E-protein family.

Submitted May 20, 2009; accepted February 22, 2010. Prepublished online as *Blood* First Edition paper, March 15, 2010; DOI 10.1182/blood-2009-05-223057.

The online version of this article contains a data supplement.

The publication costs of this article were defrayed in part by page charge payment. Therefore, and solely to indicate this fact, this article is hereby marked "advertisement" in accordance with 18 USC section 1734.

This family of transcription factors recognizes a consensus DNA sequence known as the E-box (CANNTG) in dimer form, whereas monomeric forms have no discernible DNA-binding activity.[21,22] The E-protein family of proteins is known to regulate lymphocyte development,[23] neural differentiation,[24] and myogenesis.[25] Our previous study demonstrated that E2-2 can inhibit the activity of VEGFR2 luciferase reporters in ECs.[26] However, how E2-2 counteracts the activity of the VEGFR2 promoter and whether E2-2 influences the actions of ECs remain veiled. In this study, we explored the role of E2-2 in angiogenesis both in vitro and in vivo. We found that E2-2 represses VEGFR2 promoter activity to inhibit angiogenesis and that E2-2–mediated EC inactivation can be alleviated through interaction with Id1.

Methods

Plasmids and adenoviruses

cDNAs for human and mouse E2-2 as well as mouse LMO2 were cloned by reverse-transcription polymerase chain reaction (RT-PCR). Each cDNA was sequenced before use. E2-2ΔHLH and Id1ΔHLH were generated by Pfx DNA polymerase (Invitrogen) using human E2-2 or mouse Id1 as templates, respectively. Mouse stem cell leukemia hematopoietic transcription factor (SCL) was a kind gift from Dr M. Ema (University of Tsukuba, Japan).[27] cDNAs were inserted into Flag-pcDNA3 or Myc-pcDNA3[28] and subsequently ligated into the pcDEF3 vector.[29] DEF3-Flag-Id1, DEF3-Myc-Id1, and DEF3-Id1 have been previously described.[20] MCKpfos-luc and pGL2b-VEGFR2-luc (−166 bp/267 bp) were generously provided by Drs M. Sigvardsson (Lund University, Sweden) and C. C. W. Hughes (University of California, Irvine), respectively.[26,30,31] VEGFR2-luc mutant constructs were also generated by PCR. After verification of each sequence, reporter constructs were used for each experiment. Adenoviruses expressing Myc-E2-2 were generated using the pAdTrack-CMV vector.[32] After recombination of pAdTrack-CMV-Myc-E2-2 with pAdEasy-1,[32] the resulting plasmid was transfected into 293T cells, and adenoviruses were amplified. Adenoviruses expressing Flag-Id1 have been reported.[20]

Cell culture

COS7 cells and mouse embryonic endothelial cells (MEECs)[17] were maintained in Dulbecco modified Eagle medium (DMEM; Invitrogen) containing 10% fetal calf serum (FCS; Invitrogen), minimum essential medium nonessential amino acids (Invitrogen), and 100 U/mL penicillin/streptomycin (Wako). Calf pulmonary aortic endothelial cells (CPAEs)[33] were cultured in DMEM with 10% FCS, 20mM N-2-hydroxyethylpiperazine-N′-2-ethanesulfonic acid (Wako), and 100 U/mL penicillin/streptomycin. Primary human umbilical vein endothelial cells (HUVECs) were cultured in endothelial basal medium (Lonza Walkersville) supplemented with 2% FCS. MEECs and HUVECs were grown on 0.1% gelatin-coated dishes.

Adenoviral infections

Adenoviruses were incubated in DMEM containing polybrene (Sigma-Aldrich; 80 μg/mL) for 2 hours and added to the dishes. Two hours after infection, cells were washed and allowed to recover 24 hours before the experiments. If necessary, cells were starved by removal from the FCS overnight and then stimulated with 50 ng/mL recombinant human VEGF (Wako).

Immunoprecipitation and Western blotting

To detect interactions among the proteins, plasmids were transfected into COS7 cells (5×10^5 cells/6-cm dish) using FuGENE6 (Roche Diagnostics). Forty hours after transfection, the cells were lysed in 500 μL of TNE buffer (10mM Tris [pH 7.4], 150mM NaCl, 1mM ethylenediamine-*N*′, *N*′, *N*′, *N*′-tetraaccetic acid, 1% NP-40, 1mM phenymethylsulfonyl-l-fluoride, 5 μg/mL leupeptin, 100 U/mL aprotinin, 2mM sodium vanadate, 40mM NaF, and 20mM β-glycerophosphate). Cell lysates were precleared with protein G-Sepharose beads (GE Healthcare) for 30 minutes at 4°C and then incubated with anti-Flag M5 antibody (Sigma-Aldrich) for 2 hours at 4°C. Protein complexes were immunoprecipitated by incubation with protein G-Sepharose beads for 30 minutes at 4°C followed by 3 washes with TNE buffer. Immunoprecipitated proteins and aliquots of total cell lysates were boiled for 5 minutes in sample buffer, separated by sodium dodecyl sulfate-polyacrylamide gel electrophoresis, and transferred to Hybond-C Extra membranes (GE Healthcare). The membranes were probed with anti-Myc 9E10 antibody (Santa Cruz Biotechnology). Primary antibodies were detected using horseradish peroxidase-conjugated goat anti–mouse antibody (GE Healthcare) and chemiluminescent substrate (Thermo Electron). Protein expression in total cell lysates was evaluated by Western blotting using anti-Flag M5 or anti-Myc 9E10 antibody. To detect the endogenous interaction between Id1 and E2-2, either an anti–E2-2 monoclonal antibody (anti-TCF4 M03; Abnova) or an anti-Id1 polyclonal antibody (Santa Cruz Biotechnology) was used.

RNA isolation and RT-PCR

Total RNA was isolated using the RNeasy kit (QIAGEN). Reverse transcription was carried out using a First-Strand cDNA Synthesis Kit (Takara). PCR was performed using Taq polymerase (Invitrogen) as directed by the manufacturer. Primer sets used are shown in supplemental Tables 1 and 2 (available on the *Blood* Web site; see the Supplemental Materials link at the top of the online article).

Transcriptional reporter assay

MEECs were seeded at 5×10^4 cells/well in 12-well plates 1 day before transfection.

Cells were transfected using Lipofectamine (Invitrogen) and Plus Reagent (Invitrogen). After 40 hours of transfection, lysates were prepared and luciferase activity was measured using a luciferase assay system (Promega). Results were corrected by measuring β-galactosidase activity (pCH110; GE Healthcare). Each experiment was carried out in triplicate and repeated at least twice. Values represent the mean plus or minus SD ($n = 3$).

Immunofluorescence

Immunofluorescence assay was performed as previously described.[34] Briefly, MEECs grown on the cover glass were stimulated with 25 ng/mL BMP6 to induce Id1. After treatment, the glasses were washed once with phosphate-buffered saline (PBS), fixed for 10 minutes with 4% paraformaldehyde (PFA; Wako), washed 3 times with PBS, subsequently permeabilized with 0.5% Triton X-100 in PBS for 5 minutes, and washed again 3 times with PBS. Glasses were blocked with 5% normal swine serum (Dako Denmark) in PBS at 37°C for 1 hour and incubated with 5% normal swine serum (in PBS) containing mouse monoclonal anti–E2-2 (anti-TCF4 M03) and rabbit polyclonal Id1 antibodies at 4°C overnight. The glasses were then washed 3 times with PBS, incubated with 5% normal swine serum (in PBS) including both fluorescein isothiocyanate-conjugated goat anti–mouse IgG antibody (diluted 1:250; Invitrogen) and Texas red-conjugated goat anti–rabbit IgG antibody (diluted 1: 250; Invitrogen) at room temperature for 1 hour, and washed 3 times with PBS. To visualize the fluorescence, an immunofluorescence microscope (Axiovert 200M; Carl Zeiss) was used.

Migration assay

Cell migration assays were performed using a Boyden chamber. Costar nucleopore filters (8-μm pore diameter) were coated with 10 μg/mL fibronectin (Sigma-Aldrich) overnight at 4°C. The chambers were washed 3 times with PBS. Adenovirus-infected HUVECs starved for 12 hours without FCS were added to the top of each migration chamber at a density of 1.5×10^4 cells/chamber in 150 μL of endothelial basal medium without FCS. Cells were allowed to migrate to the underside of the chamber in the presence or absence of 50 ng/mL VEGF in the lower chamber. After

6 hours, cells were fixed in 4% PFA and stained with 0.5% crystal violet (dissolved in 25% methanol; Wako). The upper surface was wiped with cotton swabs to remove nonmigrating cells. Cells present on the lower surface were counted. Each experiment was carried out in triplicate and repeated several times. Values represent the mean plus or minus SD (n = 3).

Network formation assay

HUVECs (2×10^4 cells/well in an 8-well Lab-Tek chamber; Thermo Electron) infected with adenoviruses were seeded on growth factor-reduced Matrigel (BD Biosciences). Ninety minutes later, images were captured every 15 minutes for 4 hours using a time-lapse microscope (Axiovert 200M; Carl Zeiss) to monitor cell behavior.

Erk phosphorylation

HUVECs were seeded at 1×10^5 cells/well in 12-well plates. Twenty-four hours after HUVECs were infected with the E2-2–expressing adenoviruses, HUVECs were starved without FCS for 12 hours. Then, HUVECs were stimulated with 50 ng/mL VEGF for the indicated times. Phospho-Erk1/2, Erk2, Myc-E2-2, and β-actin were analyzed by Western blots of total cell lysates using antiphospho-Erk(p44/p42) (Cell Signaling), anti-Erk2 (Santa Cruz Biotechnology), anti-Myc9E10 (Santa Cruz Biotechnology), and anti–β-actin (Sigma-Aldrich) antibodies, respectively.

Cell proliferation

Proliferation was measured by direct counting of cultures in 12-well plates. CPAEs were seeded at 1×10^4 cells/well in 12-well plates 1 day before adenoviral infection. We began counting cells 1 day after adenoviral infection.

Mouse angiogenesis assay

The formation of new vessels in vivo was evaluated by Matrigel plug assay with some modifications to the previously described method.[35] Adenoviruses expressing 1×10^9 pfu of green fluorescent protein (GFP), 1×10^9 pfu of E2-2, and/or 2.5×10^8 pfu of Id1 were mixed in the Matrigel solution at 4°C with 200 ng/mL VEGF-A (Wako), 1 μg/mL bFGF (R&D Systems), and 100 μg/mL heparin (Wako). A total of 500 μL of Matrigel-containing adenoviruses was injected subcutaneously into the abdomen of male ICR mice. The mice were killed 7 days after the injection. The Matrigel plugs with adjacent subcutaneous tissues were recovered by en bloc resection, and images were then taken using a stereomicroscope (Leica). Thereafter, each sample was embedded in the optimal cutting temperature (OCT) compound and quickly frozen in liquid nitrogen to be sectioned at a thickness of 5 μm at −18°C. After being fixed with 4% PFA/PBS, anti–rat monoclonal PECAM-1 antibody (1:200 dilution) was used as a primary antibody. Then, the sections were incubated with Alexa568-conjugated goat anti–rat IgG antibody (1:200 dilution; Invitrogen). Images were taken using a fluorescence microscope (Carl Zeiss). Mice were housed in the animal facilities of Laboratory Animal Resource Center in University of Tsukuba under specific pathogen-free conditions with constant temperature and humidity and fed a standard diet. Treatment of mice was approved by the Animal Care and Use Program at the University of Tsukuba.

Knock-down of E2-2

The pLVTHM lentiviral vector for shRNA was purchased from Addgene. Double-strand DNAs for 5′-cgcgtcccc**AGAGCTGAGTGATTTACT**-GttcaagagaCAGTAAATCACTCAGCTCTtttttggaaat/3′-aggggTCTCGACT-CACTAAATGACaagttctctGTCATTTAGTGAGTCGAGAaaaaaccttagc-5′ (shE2-2#1) and 5′-cgcgtcccc**GAAATTAGATGACGACAAG**ttcaagaga-CTTGTCGTCATCTAATTTCtttttggaaat-3′/3′-aggggCTTTAATCTACT-GCTGTTCaagttctctGAACAGCAGTAGATTAAAGaaaaaccttagc-5′ (shE2-2#4) were inserted into pLVTHM digested with both MluI and ClaI. Lentiviral vectors expressing shE2-2 were transfected into 293T cells together with psPAX2 and pMD2.G. The lentiviruses were incubated for 2 hours in DMEM containing polybrene (80 μg/mL) and then added to the dishes. Two hours after being infected, the cells were washed and cultured in medium. Infected HUVECs, which became GFP-positive, were isolated by fluorescence-activated cell sorting and used for the experiments.

Results

Identification of Id1-interacting proteins

To obtain insight into how Id1 activates angiogenesis, we isolated proteins that interact with Id1 using a yeast 2-hybrid system. We used Id1 as bait to screen an amplified human aorta cDNA library (with an original complexity of 3.5×10^6 independent cDNA clones). Among the positive clones identified, the cDNA encoding E2-2 was isolated most frequently. We then investigated whether E2-2 interacts with Id1 in mammalian cells. We also tested the interaction of E2-2 with Herp2, LMO2, and SCL, which are known to modulate EC activation.[20,36-38] As shown in Figure 1A, E2-2 interacted with Id1, SCL,[26] and itself, but not with Herp2 or LMO2. In the reciprocal experiment, Id1 bound strongly with E2-2 and marginally with LMO2 and itself (Figure 1B). When the membrane was exposed for a longer time, an interaction between Id1 and Herp2, which we have described previously,[20] was observed (data not shown). These results indicated that the interaction between Id1 and E2-2 is the most prominent of the combinations tested.

To confirm that the interaction between E2-2 and Id1 is physiologically significant, we investigated the interaction between endogenous proteins in MEECs stimulated with BMP6 for 3 hours because Id1 is known to be induced by BMPs.[39] After cell lysis, immunoprecipitation was performed using an anti–E2-2 antibody. Subsequently, immunoprecipitates were blotted with an anti-Id1 antibody. As shown in Figure 1C, endogenous Id1 formed a complex with endogenous E2-2 in cells. Conversely, the specific band corresponding to E2-2 could be detected (arrow) when cell lysates were immunoprecipitated with an anti-Id1 antibody (supplemental Figure 1). The interaction between E2-2 and Id1 led us to investigate whether E2-2 colocalizes with Id1. To show colocalization of E2-2 with Id1 in ECs, subcellular localization was determined with a fluorescence microscopy by staining E2-2 with fluorescein isothiocyanate-conjugated goat anti–mouse IgG and Id1 with Texas Red-conjugated goat anti–rabbit IgG. E2-2 and Id1 colocalized in nucleus (Figure 1D), which is consistent with an interaction between the 2 proteins. In addition, we used the aorta ring assay to visualize the expressions of E2-2 and Id1 with fluorescent imaging. When both E2-2 and Id1 were costained with fluorescence probes, we recognized that both proteins in sprouting ECs could colocalize in the nucleus (data not shown).

HLH domains play an important role in protein-protein interactions. To examine the contribution of HLH domains to the E2-2/Id1 interaction, we made E2-2 and Id1 mutants lacking the respective HLH domains (supplemental Figure 2A). As shown in supplemental Figure 2B and C, E2-2 did not interact with E2-2ΔHLH or Id1ΔHLH. Similarly, Id1 did not interact with E2-2ΔHLH (supplemental Figure 2D). To further confirm that the HLH domain of E2-2 is enough for E2-2 to interact with Id1, we made an expression construct for GFP, which was fused with the HLH domain derived from E2-2 (GFP-HLH). When GFP-HLH was cotransfected with Id1 in COS7 cells, we could observe the interaction between GFP-HLH and Id1 (supplemental Figure 2E). However, its interaction seemed to be weak. Thus, the other domain(s) of E2-2, except for its HLH domain, might contribute to the adequate interaction between E2-2 and Id1. Taken together, these results indicated that E2-2 heterodimerizes with Id1 and

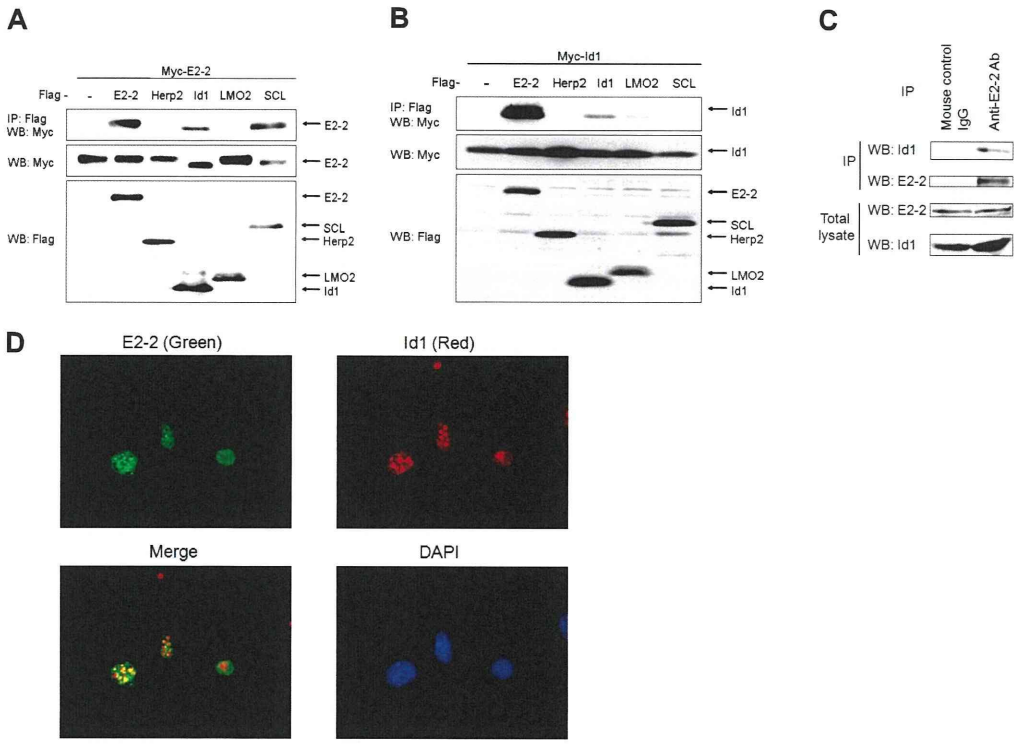

Figure 1. Interaction between E2-2 and Id1. (A) Interaction of Myc-E2-2 with Flag-Id1. Myc-E2-2 was cotransfected with Flag-E2-2, Flag-Herp2, Flag-Id1, Flag-LMO2, or Flag-SCL. Immunoprecipitations were carried out using anti-Flag M5 antibody, and coimmunoprecipitated E2-2 was detected by Western blotting using anti-Myc 9E10 antibody (top panel). The expression of Myc-E2-2 and proteins conjugated with Flag at the N-terminus was evaluated using anti-Myc 9E10 (middle panel) and anti-Flag M5 antibodies (bottom panel), respectively. (B) Interaction of Myc-Id1 with Flag-E2-2. The experiment was performed in a manner similar to that described in panel A. Interaction of Myc-Id1 with Flag-tagged proteins (top panel). Expression of Myc-Id1 and Flag-tagged proteins was checked using anti-Myc 9E10 antibodies (middle panel) and anti-Flag M5 antibodies (bottom panel), respectively. (C) Endogenous interaction between Id1 and E2-2. MEECs were stimulated with BMP6 for 3 hours. Cell lysates were immunoprecipitated with a mouse anti–E2-2 monoclonal antibody, followed by Western blotting with a rabbit anti-Id1 polyclonal antibody (top panel). Expression of E2-2 in immunoprecipitates was checked using an anti–E2-2 monoclonal antibody (second panel). To show expression of E2-2 and Id1 in total lysates, an anti–E2-2 monoclonal antibody (third panel) and an anti-Id1 polyclonal antibody (bottom panel) were used. As a negative control, mouse control IgGs were used for immunoprecipitation. (D) Colocalization of E2-2 with Id1 in MEECs. MEECs were stained with a mouse anti–E2-2 monoclonal antibody (green) or a rabbit anti-Id1 polyclonal antibody (red). Nuclei were visualized using 4′,6-diamidino-2-phenylindole. After samples were mounted with Fluorescent Mounting Medium (Dako Denmark), they were visualized using an immunofluorescence microscope (Axiovert 200M; Carl Zeiss) with a 63×/1.4 oil objective lenses (Carl Zeiss). Images were acquired with AxioCam MRm 60-C1 (Carl Zeiss) and processed with the AxioVision Rel 4.4 (Carl Zeiss) and Adobe Photoshop 7.0.1 software (Adobe).

homodimerizes through its HLH domain. In addition, Id1 requires its HLH domain to associate with E2-2.

Inhibition of E2-2–mediated transcription by Id1

The MCKpfos-luc reporter construct consisting of 4 E-box elements has been used to investigate the function of E-proteins.[26,30] E2-2 enhanced the activity of this reporter in a dose-dependent manner (supplemental Figure 3A), but E2-2ΔHLH was unable to potentiate reporter activity (data not shown). Id proteins have been reported to interact with bHLH transcription factors and prevent them from binding to DNA or forming active heterodimers (or homodimers).[3] Although we did not know whether E2-2 forms a homodimer or a heterodimer with other bHLH proteins in MEECs to activate this reporter, Id1 blocked E2-2–induced reporter activity as anticipated (Figure 2A; supplemental Figure 3B). Consistent with the undetectable interaction between E2-2 and Id1ΔHLH, E2-2–induced reporter activity was not reduced by Id1ΔHLH (Figure 2A).

As we have reported,[26] E2-2 inhibited VEGFR2 reporter activity in MEECs in a dose-dependent manner (supplemental Figure 3C), whereas the introduction of Id1 into MEECs relieved the E2-2–mediated repression (Figure 2B). To show that Id1 indeed hampers E2-2 dimer formation, COS7 cells were cotransfected with Myc-E2-2 and Flag-E2-2 in the absence or presence of Myc-Id1. Immunoprecipitation of COS7 cell extracts revealed that Id1 blocked E2-2 homodimer formation (Figure 2C). We also investigated whether Id1 can disrupt the preexisting E2-2 homodimer. We prepared lysates from cells transfected with either Myc-Id1 or pcDNA3. Subsequently, each lysate was mixed with lysate prepared from cells transfected with both Myc-E2-2 and Flag-E2-2, immunoprecipitated with anti-Flag antibody, and then analyzed by Western blotting with anti-Myc antibody. As seen in Figure 2D, Id1 could efficiently make the preexisting E2-2 homodimer dissociated.

Inhibition of EC activation by E2-2

We speculated that E2-2 would have an opposite effect on EC activation compared with Id1 because Id1 antagonized E2-2–mediated reporter activity. To investigate the effect of E2-2 on network formation, we infected HUVECs with either GFP- or E2-2–expressing adenoviruses before seeding the cells on Matrigel. We then observed the formation of cord-like structures by time-lapse microscopy (Figure 3A). As seen in video (supplemental Figure 4A-B), HUVECs expressing E2-2 did not form cord-like structures as quickly as HUVECs expressing GFP as a control did. We also investigated the effect of E2-2 on cell migration in the presence of VEGF. HUVECs challenged with VEGF after infection with E2-2–expressing adenoviruses exhibited decreased migration

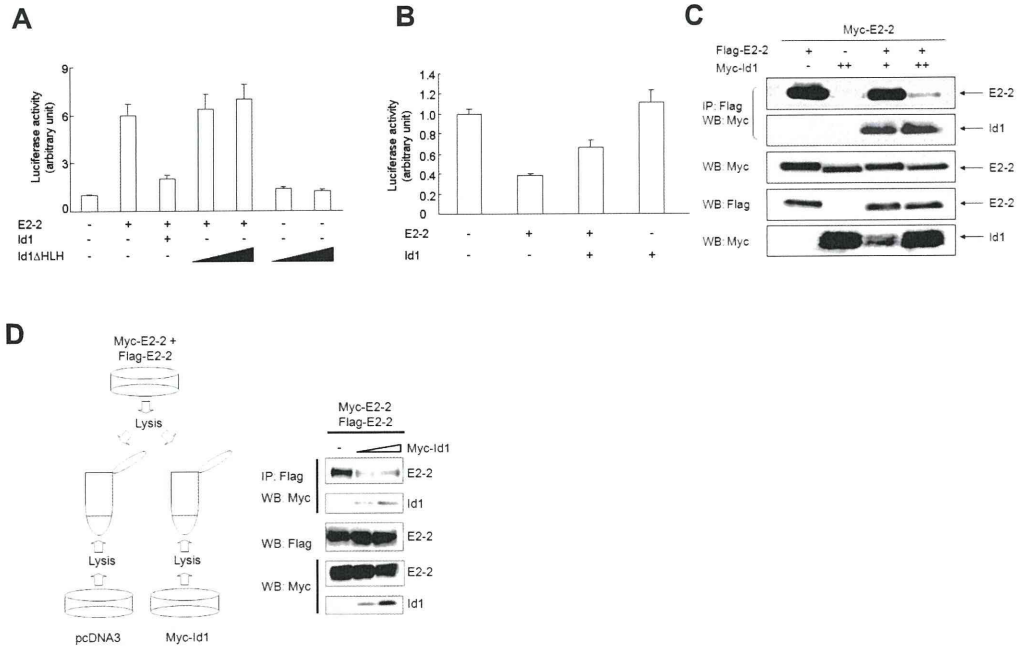

Figure 2. Id1 counteracts E2-2–mediated luciferase activity. (A) Id1ΔHLH does not perturb E2-2–induced MCKpfos-luc activity. MEECs were transfected with MCKpfos-luc, E2-2, and either Id1 or different amounts of Id1ΔHLH. (B) Id1 relieves the inhibition of pGL2b-VEGFR2-luc (−166 bp/267 bp) activity by E2-2. MEECs were transfected with pGL2b-VEGFR2-luc (−166 bp/267 bp), Id1, and E2-2. (C) Id1 disrupts E2-2 homodimer formation. The experiment was performed as described in Figure 1A. E2-2 homodimer formation (top panel) and E2-2/Id1 heterodimer formation (second panel) are shown. Expressions of Myc-E2-2 (third panel) and Myc-Id1 (bottom panel) were evaluated using an anti-Myc 9E10 antibody, and the expression of Flag-E2-2 was shown using an anti-Flag M5 antibody (fourth panel). (D) Id1 disturbs the preexisting E2-2 homodimer formation. Left panel: Illustration of how cell lysates were prepared from each dish in which indicated plasmids were transfected in COS7 cells. Right panel: After each cell lysate was mixed, the experiment was performed as described in Figure 1A. E2-2 homodimer formation (top panel) and E2-2/Id1 heterodimer formation (second panel) are shown. The expression of Flag-E2-2 was shown using an anti-Flag M5 antibody (third panel). Expressions of Myc-E2-2 (fourth panel) and Myc-Id1 (bottom panel) were evaluated using an anti-Myc 9E10 antibody.

compared with cells infected with GFP-expressing adenoviruses (Figure 3B). Because Id1 perturbs the function of E2-2, we examined the possibility that Id1 would relieve the E2-2–mediated repression of the VEGF-induced chemotactic response. Indeed, Id1 marginally rescued the inhibitory effect of E2-2 on VEGF-induced cell migration (Figure 3B). Importantly, VEGF-induced HUVEC migration was also increased when E2-2 levels were decreased via lentiviral expression of human shE2-2s but not in response to control lentiviruses (Figure 3C).

Impairment of in vivo angiogenesis by E2-2

Because E2-2 inhibits EC activation in vitro, we tried to examine whether in vivo angiogenesis would be affected by overexpression of E2-2. To elucidate this possibility, we used the Matrigel plug assay by which the angiogenic (or antiangiogenic) ability of proteins, cytokines, or compounds can be assigned. To overexpress E2-2 and/or Id1, we subcutaneously injected Matrigel mixed with E2-2– and/or Id1-expressing adenoviruses.[35,40] Seven days after implantation of the Matrigel plugs together with adenoviruses expressing E2-2 and/or Id1, the Matrigels were removed. When we investigated whether the protein expression by the method of adenoviral gene transfer was kept for 7 days, GFP-positive cells were detected in the Matrigel plugs (supplemental Figure 5). As seen in Figure 4A, there were fewer blood vessels observed in the Matrigel plugs containing E2-2–expressing adenoviruses than in those containing control adenoviruses. Because Id1 influenced the E2-2–mediated inhibition of EC activation, we mixed the Id1-expressing adenoviruses with E2-2–expressing adenoviruses and injected them into the Matrigel plugs implanted under the skin. As expected, the injection of Id1-expressing adenoviruses restored in vivo angiogenesis suppressed by E2-2. When the cells expressing PECAM-1 were visualized using the frozen sections, there were fewer PECAM-1–positive cells seen in the Matrigel plugs injected with adenoviruses expressing E2-2 than in those injected with control adenoviruses or a combination of Id1-expressing adenoviruses with E2-2–expressing adenoviruses (Figure 4B-C). These results indicated that, in contrast to Id1, E2-2 is an antagonistic molecule for angiogenic reaction.

To investigate the mechanism by which E2-2 inhibits angiogenic reaction both in vitro and in vivo, we examined the expression of several genes known to be implicated in angiogenesis (eg, VEGFR1, VEGFR2, VEGF, PECAM-1, and VE-cadherin). Of the genes examined, VEGFR2 mRNA was considerably reduced in both human and bovine ECs after infection with E2-2–expressing adenoviruses (Figure 4D); the expression of VEGF was marginally decreased by E2-2. VEGFR1, PECAM-1, and VE-cadherin mRNA levels, however, did not change in response to E2-2 overexpression (Figure 4D). Because VEGFR2 mRNA was prominently decreased by E2-2, we were prompted to check its protein expression after the infection of E2-2 to HUVECs. Consistent with the result of VEGFR2 mRNA expression, E2-2 slightly inhibited the expression of VEGFR2 protein, whereas Id1 partially rescued decrease of VEGFR2 protein mediated by E2-2 (supplemental Figure 6B).

VEGF signaling through the activation of the VEGFR2 receptor elicits multiple effects on ECs, such as migration, proliferation, survival, and differentiation.[41] One of the signaling pathways downstream of VEGF/VEGFR2 is the MAP kinase pathway. When HUVECs were stimulated with VEGF, Erk was transiently phosphorylated (Figure 4E). Its phosphorylation peaked at 10 minutes after VEGF stimulation and declined rapidly thereafter. When E2-2 was overexpressed in HUVECs

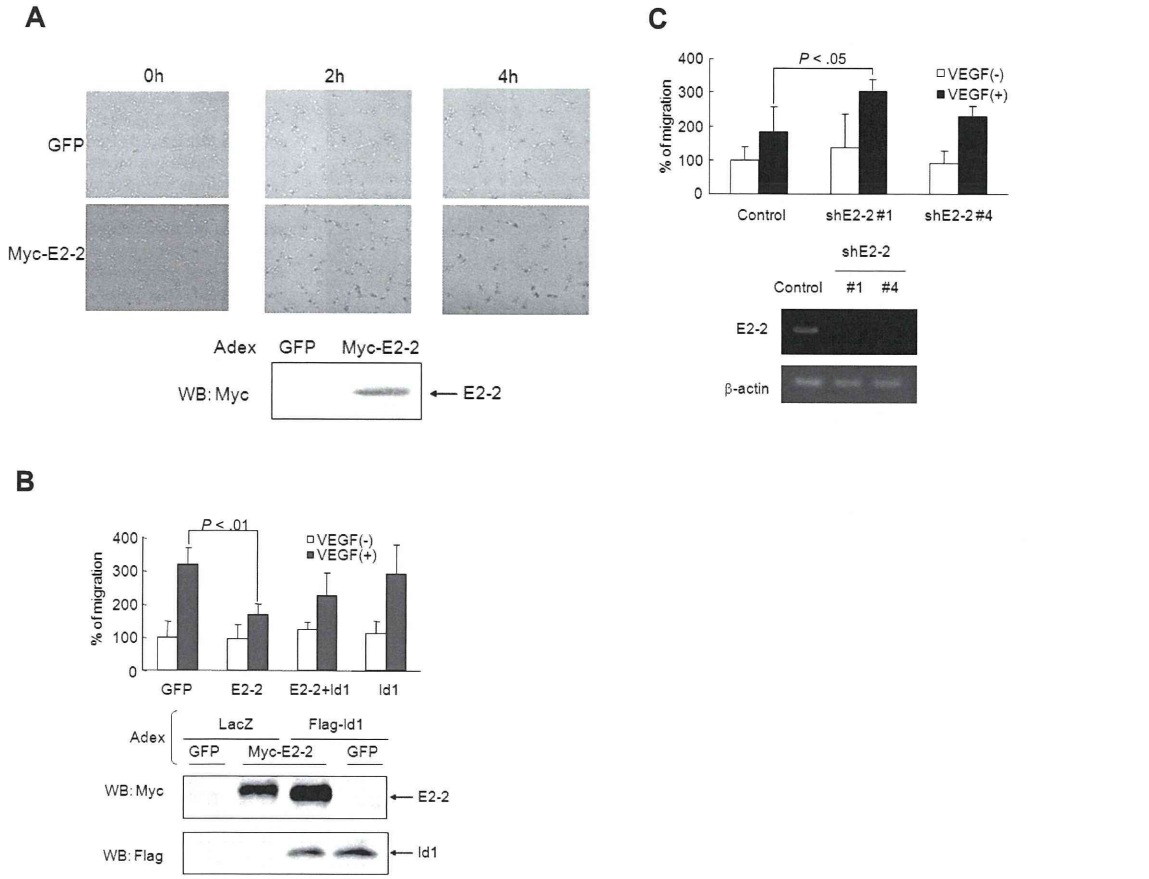

Figure 3. E2-2 blocks EC activation. (A) E2-2 inhibits the formation of cord-like structures on the Matrigel. Forty hours after adenoviral infection, HUVECs were seeded on the Matrigel. Ninety minutes later, images were recorded every 15 minutes by time-lapse microscopy (supplemental Figure 4A-B). The images at 0-, 2-, and 4-hour time points are shown. Bottom panel: Expression of Myc-E2-2. Samples were visualized using a conventional microscope (Axiovert 200M; Carl Zeiss) with a 5×/0.12 dry objective lenses (Carl Zeiss). Images were acquired with AxioCam MRm 60-C1 (Carl Zeiss) and processed with the AxioVision Rel 4.4 (Carl Zeiss) and Adobe Photoshop 7.0.1 software (Adobe). (B) Id1 rescues E2-2–mediated inhibition of cell migration. After adenoviral infection, HUVECs were seeded on the upper membrane of the Boyden chamber. VEGF (50 ng/mL) was added to the lower chamber. After 6 hours, cells were stained with crystal violet, and the number of transmigrated cells was counted. Adenoviruses expressing LacZ or GFP were used as controls. Values represent the mean plus or minus SD (n = 3). Bottom panels: Myc-E2-2 and Flag-Id1 expression levels. Significant difference was calculated by the Student *t* test. (C) shE2-2 enhances VEGF-induced effect on HUVEC migration. Lentiviruses expressing GFP alone, shE2-2#1, or shE2-2#4 were infected in HUVECs. After sorting lentivirus-infected cells using GFP as a marker, sorted HUVECs were used for migration assay as described in panel B. Bottom panels: Expressions of E2-2 and β-actin by RT-PCR. Values represent the mean plus or minus SD (n = 3). Significant difference was calculated by the Student *t* test.

by adenoviral gene transfer, VEGF induced phosphorylation of Erk with similar kinetics to those of HUVECs infected with GFP-expressing adenoviruses; however, the extent of Erk phosphorylation was diminished (Figure 4E-F). Consistent with the inhibition of VEGF-induced Erk phosphorylation by E2-2, CPAEs and HUVECs expressing E2-2 proliferated more slowly than those expressing GFP (Figure 4G; supplemental Figure 6C). Taken together, these observations support the idea that E2-2 has the ability to inhibit EC activation by antagonizing VEGF signaling.

Id1 has been implicated in the regulation of the expression of integrin α6, integrin β4, FGFR1, MMP2, and laminin5; loss of Id1 results in decreased protein levels.[19] Because Id1 antagonizes the function of E2-2, we hypothesized that genes suppressed transcriptionally by the loss of Id1 might be negatively regulated by E2-2. Transcript levels of MMP2 and integrin β4, but not of other genes, in ECs were reduced by overexpression of E2-2 (Figure 4D; and data not shown). Thus, E2-2 may also block EC activation through transcriptional repression of other proangiogenic genes.

Suppression of VEGFR2 promoter by E2-2

Because ectopic E2-2 reduced VEGFR2 mRNA levels in ECs (Figure 4D), we tried to determine which regions of the VEGFR2 promoter could be affected by E2-2. We tested several VEGFR2 promoter constructs truncated downstream of position −166 for E2-2 responsiveness. Basal reporter activity was greatly reduced on removal of the sequence between −80 and −40. However, all of the constructs were strongly inhibited by E2-2 in a dose-dependent manner (Figure 5A). Two typical E-boxes located in the 5′ noncoding region of the VEGFR2 gene were predicted to be involved in the inhibition of VEGFR2 promoter activity by E2-2. To test this hypothesis, we made 7 3′-truncation mutants of the VEGFR2 promoter (Figure 5B). Basal reporter activity gradually decreased as the 5′ noncoding region was truncated. Unexpectedly, E2-2 could still attenuate the luciferase activity even when both E-boxes were deleted. Furthermore, the activity of pGL2b-VEGFR2-luc (−40 bp/5 bp) was also inhibited by E2-2 despite very low basal luciferase activity. GATA-1 and/or GATA-2 are known to positively regulate VEGFR2 promoter activity by binding to the 5′ noncoding region (98-122 bp).[42] However, the basal activity of the reporter lacking the GATA binding site (pGL2b-VEGFR2-luc [-80 bp/93 bp]) remained at 60% of the reporter activity with the binding site included (pGL2b-VEGFR2-luc, −80 bp/159 bp). Thus, it appears that neither GATA sequences nor E-boxes are required for E2-2 to repress the activity of the VEGFR2 promoter.

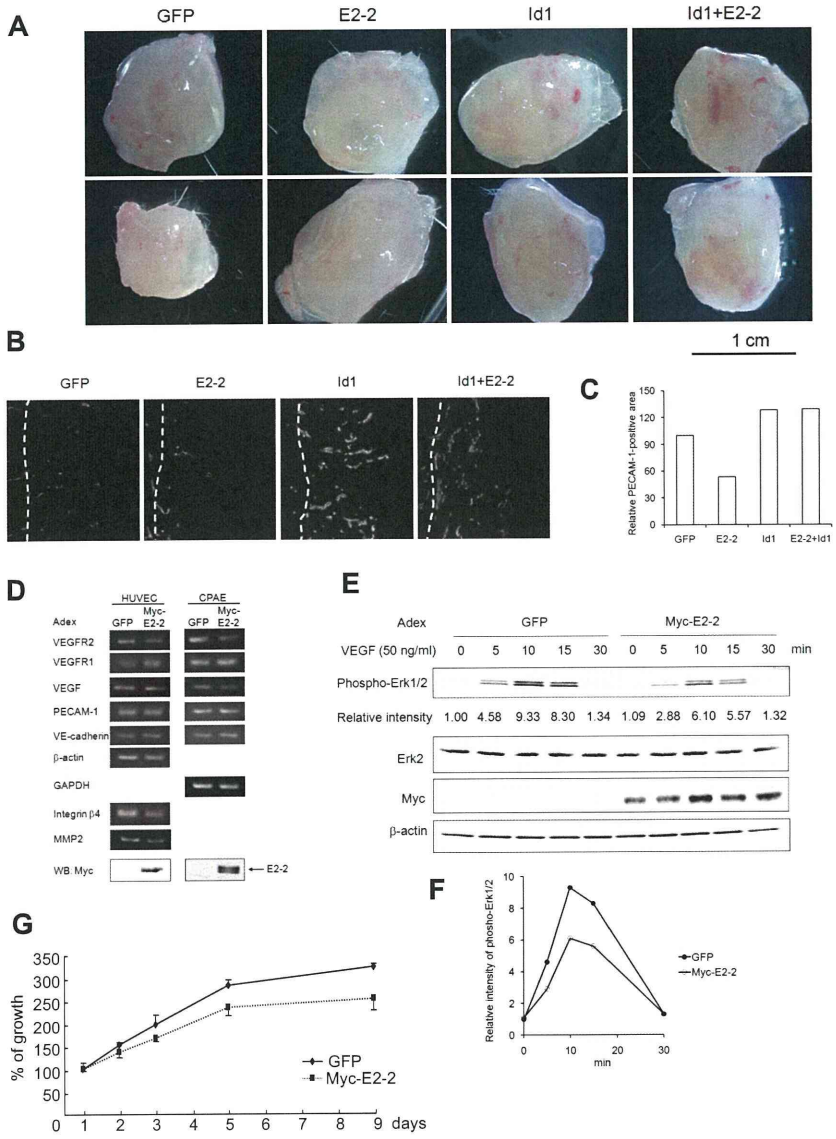

Figure 4. Suppression of angiogenesis by E2-2. (A) Photographs for en bloc resection, including Matrigel plugs with adjacent subcutaneous tissues. Samples were visualized using a stereomicroscope (S8APO; Leica). Images were acquired with EC3 (Leica) and processed with the LAS EZ (Leica) and Adobe Photoshop 7.0.1 software (Adobe). (B) PECAM-1 staining of frozen sections. Matrigels are located to the right side of broken lines, whereas there are mouse subcutaneous tissues to the left side of broken lines. PECAM1-positive areas are shown as white. After samples were mounted with Fluorescent Mounting Medium (Dako Denmark), they were visualized using an immunofluorescence microscope (Axiovert 200M; Carl Zeiss) with a 63×/1.4 oil objective lenses (Carl Zeiss). Images were acquired with AxioCam MRm 60-C1 (Carl Zeiss) and processed with the AxioVision Rel 4.4 (Carl Zeiss) and Adobe Photoshop 7.0.1 software (Adobe). (C) Relative PECAM-1-positive area in Matrigel plugs. Five fields were randomly chosen in each condition from panel B, and PECAM-1-positive areas were scored using the imaging software. PECAM-1-positive areas were normalized with the areas of the field. Each relative PECAM-1-positive area was calculated by the comparison of the score in Matrigel plugs, including GFP. (D) Effect of E2-2 on the expression of mRNAs implicated in EC activation. mRNAs involved in EC activation were analyzed by RT-PCR. HUVECs or CPAEs were infected with adenoviruses expressing E2-2 or GFP as a negative control. Gene transcript names are indicated to the left of the figure. mRNAs for β-actin and GAPDH were included as internal controls. The expression of Myc-E2-2 was evaluated in total cell lysates using an anti-Myc 9E10 antibody (bottom panel). Adex indicates adenovirus. To show that EC markers are expressed in CPAEs, RT-PCR was carried out (supplemental Figure 6A). (E) E2-2 inhibits VEGF-induced Erk phosphorylation. Phospho-Erk1/2 (top panel), Erk2 (second panel), Myc-E2-2 (third panel), and β-actin (bottom panel) levels were analyzed by Western blots of total cell lysates. Adenoviruses expressing GFP were used as a negative control. The expression for phosphorylation of Erk1/2 was normalized using the intensity of the band corresponding to Erk2. Each relative intensity was calculated by the comparison of the value for cells infected with GFP-expressing adenoviruses in the absence of VEGF. (F) Graphical presentation for relative intensity of phospho-Erk1/2 levels in panel E: ● represents GFP-expressing adenoviruses; ○, Myc-E2-2–expressing adenovirusues. (G) E2-2 perturbs EC proliferation. Each experiment was performed in triplicate and repeated a few times. Values represent the mean plus or minus SD (n = 3).

We next explored the effect of Id1 on the E2-2–mediated repression of VEGFR2 promoter activity. For this purpose, we used pGL2b-VEGFR2-luc (−80 bp/5 bp) instead of pGL2b-VEGFR2-luc (−40 bp/5 bp) because the basal activity of pGL2b-VEGFR2-luc (−40 bp/5 bp) was quite low. Similar to the effect of Id1 on the pGL2b-VEGFR2-luc (−166 bp/267 bp) reporter (Figure 2B), Id1 relieved the E2-2–mediated repression of pGL2b-VEGFR2-luc (−80 bp/5 bp) activity (Figure 5C), but Id1ΔHLH did not (data not shown). This evidence further convinced us that E2-2 negatively regulates the VEGFR2 promoter. Because the HLH domain of E2-2 is required to activate the MCKpfos-luc reporter (data not shown), we also tested the effect of E2-2ΔHLH on the activity of the VEGFR2 promoter. As expected, E2-2ΔHLH was not capable of inhibiting VEGFR2 promoter activity (data not shown). To test the possibility that E2-2 can bind to the VEGFR2 promoter (from −40 to 5), we performed electrophoresis mobility shift assay using glutathione S-transferase (GST) fusion proteins. GST or GST-Id1 showed no specific binding to the VEGFR2 promoter. However, a specific shifted band appeared when GST-E2-2 was mixed with the probe. Interestingly, the shifted complex decreased when GST-Id1 was added to the mixture containing GST-E2-2 and the probe (supplemental Figure 7A). To further confirm that Id1 promotes the dissociation of E2-2 from the VEGFR2 promoter, we carried out chromatin immunoprecipitation analysis using HUVECs infected with E2-2– and/or Id1-expressing adenoviruses. In the presence of Id1, the VEGFR2 promoter showed decrease in E2-2 binding (supplemental Figure 7B). These results support the data that Id1 rescues E2-2–mediated repression of VEGFR2 promoter activity.

Discussion

It is widely accepted that ubiquitous bHLH proteins, such as E2-2 and E2A, interact with tissue-restricted bHLH proteins to bind consensus E-box sequences and activate transcription of target genes. E-proteins are pivotal in the regulation of cell proliferation and differentiation. For example, E2-2 and its family member E2A play critical roles in B-cell development and perturbed T-cell development.[43-45] In the present study, we found that E2-2 could inhibit angiogenesis in Matrigel plugs implanted under the skin,

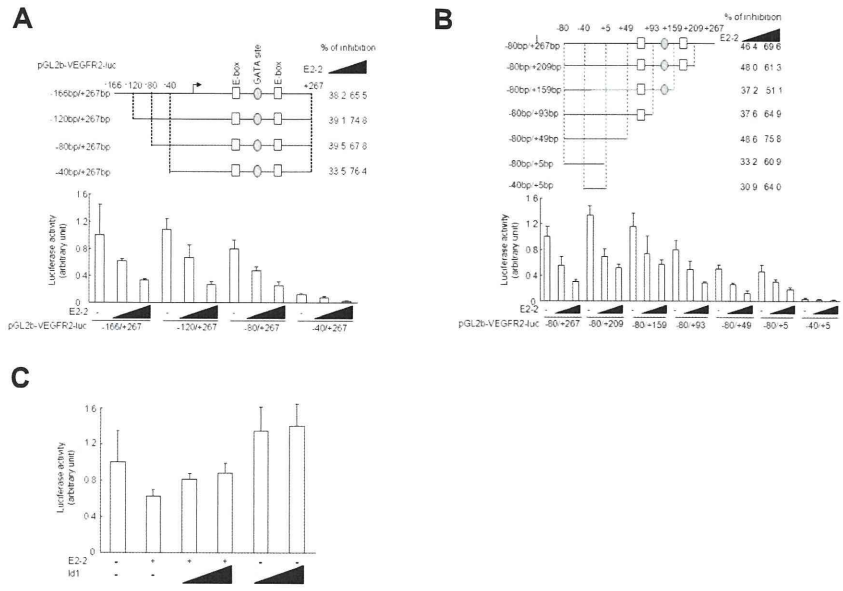

Figure 5. Analysis of the VEGFR2 promoter. (A) Effect of E2-2 on 5′ deletion mutants of the VEGFR2 promoter. MEECs were transfected with 1 of the indicated reporters with different amounts of E2-2. The inhibition percentage of reporter activities by E2-2 is indicated to the right of the top panel. (B) Effect of E2-2 on 3′ deletion mutants of the VEGFR2 promoter. The experiment was carried out as described in panel A. (C) Effect of Id1 on E2-2–mediated suppression of VEGFR2 promoter activity. Different amounts of Id1 (0.1 and 0.5 pg) were transfected together with E2-2. The experiment was carried out as described in panel A.

whereas Id1 overcame E2-2–mediated antagonism of angiogenesis in vivo.

We showed that E2-2 associated with Id1 in MEECs (Figure 1C; supplemental Figure 1A). Consistent with this interaction, Id1 blocked the E2-2–induced activity of the artificial E-box–containing reporter (MCKpfos-luc) in a manner dependent on the HLH domains of Id1 (Figure 2A; supplemental Figure 3B). On the other hand, E2-2 blocked the VEGFR2 reporter activity in ECs independently of typical E-box sequences (Figure 5B).[26] Although E2-2 generally activates the transcription of target genes by forming dimers with other bHLH proteins, a few reports have shown that E2-2 can interfere with transcription.[46,47] In the present study, we clarified that E2-2 negatively regulated the activity of the VEGFR2 promoter, which does not possess typical E-box sequences. However, the VEGFR2 promoter from −40 to 5 contains one imperfect E-box sequence (CANNTC), which has been identified as one of the binding sites of E2-2.[46] It is possible that E2-2 negatively regulates the transcription of the VEGFR2 gene through its binding to the imperfect E-box sequence because GST-E2-2 could make a specific complex with this promoter region. Excepting that possibility, E2-2 might displace TFII-I from the initiator (inr) sequences or interact with TFII-I on inr sequences to prevent TFII-I from activating transcription because TFII-I was recently found to enhance VEGFR2 transcription in an inr-dependent fashion.[48] Further investigation is needed to examine in detail how E2-2 inhibits VEGFR2 promoter activity. In an analogous fashion to E2-2, we found that E2A potentiated and inhibited MCKpfos-luc activity and VEGFR2-luc activity, respectively (supplemental Figure 8A-B), and also interacted with Id1 (supplemental Figure 8C). Furthermore, Id1 perturbed E2A-induced MCKpfos-luc activity (supplemental Figure 8A). These observations provide further evidence that E-protein family members interfere with EC activation. The mechanism by which Id1 potentiates EC activation has not been fully explored. Our study demonstrates one possible mechanism by which Id1 enhances EC activation: by antagonizing the inhibitory function of E2-2 on VEGFR2 promoter activity (supplemental Figure 9).

A number of transcription factors, such as SCL, Ets, Sp1, and NF-κB, have been identified as positive regulators of the VEGFR2 promoter.[49-52] E2-2 may also modulate the activity of these transcription factors, although the sequences between −40 and 5 of the VEGFR2 promoter are critical for the ability of E2-2 to negatively regulate VEGFR2 promoter activity.

The mRNA expressions of integrin β4 and MMP2, both of which are thought to be involved in EC activation, are reduced on ablation of the Id1 gene in cells.[19] As expected, overexpression of E2-2 in ECs down-regulated the transcripts of integrin β4 and MMP2 (Figure 4D). Hey1/Herp2/Hesr1 has been shown to inhibit the activity of both the MMP2 and the VEGFR2 promoters via the inr element.[31] The inhibition of MMP2 transcription by E2-2 might also occur via inr sequences in the MMP2 promoter. Genes other than VEGFR2, integrin β4, and MMP2 that contribute to EC activation may also be negatively regulated by E2-2. We are currently searching for such genes by DNA microarray or chromatin immunoprecipitation (ChIP-on-ChIP) analysis.

The present study demonstrated that E2-2 affects EC activation through suppression of the VEGFR2 transcript as one of its inhibitory actions. The antagonistic actions of E2-2 on EC activation were not so strong that we could exclude other possible explanations for why E2-2 blocks in vivo angiogenesis. Thus, it is possible that E2-2 also possesses the ability to influence vascular smooth muscle cells in addition to ECs to perturb angiogenic reaction in vivo. Therefore, we need to further investigate the action of E2-2 on vascular smooth muscle cells.

The addition of Id1 restored E2-2–mediated inhibition of angiogenesis. E2-2 is ubiquitously expressed, whereas Id1 is induced by a number of proangiogenic factors.[3] The function of Id1 can also be regulated by the subcellular localization during angiogenesis.[53] Thus, the balance between E2-2 and Id1 in the nucleus might determine either the activation or the resolution phase in ECs. It is possible that a compound that enhances the expression of E2-2 in ECs might provide an effective drug to inhibit tumor angiogenesis.

Recently, Deleuze et al reported that E2A (also known as E12/E47) together with SCL and LMO2 could up-regulate VE-cadherin expression to potentiate EC activation.[38] The E2-2–mediated EC suppression observed in our present study conflicts with that report. However, in their report, E2A alone did not enhance VE-cadherin expression, although the knock-down of E2A did inhibit VE-cadherin expression.[38] Furthermore, there is no